Graph-Based File Dispatching Protocol with D2D-Aided UAV-NOMA Communications in Large-Scale Networks

Baoji Wang*†, Rongqing Zhang‡§, Chen Chen*, Xiang Cheng*†, and Liuqing Yang¶
*State Key Laboratory of Advanced Optical Communication Systems and Networks, Department of Electronics, School of Electronics Engineering and Computer Science, Peking University, Beijing, China.
†Key Laboratory of Wireless Sensor Network & Communication, Shanghai Institute of Microsystem and Information Technology, Chinese Academy of Sciences, 865 Changning Road, Shanghai 200050, China.
‡School of Software Engineering, Tongji University, Shanghai 201804, China.
§National Mobile Communications Research Laboratory, Southeast University, China.
¶Department of Electrical & Computer Engineering, Colorado State University, CO, USA.

***Abstract*—Unmanned aerial vehicle (UAV)-assisted communications are expected to become an important part of the next generation mobile communication systems, due to the high mobility of the UAVs. Non-orthogonal multiple access (NOMA) is regarded as a rosy technology in the fifth generation (5G) mobile communication systems, since it can effectively improve the spectral efficiency. In this paper, we combine the advantages of the UAV-assisted communications and NOMA, and propose a device-to-device (D2D)-enhanced UAV-NOMA network architecture, in which D2D is introduced to increase the file dispatching efficiency. Resource reuse based on spatial reuse is also allowed to further improve the spectral efficiency. Then, we propose a graph-based file dispatching (GFD) protocol to control the interference and minimize the UAV-assisted file dispatching mission time. Simulation results verify the advantages of our proposed D2D-enhanced UAV-NOMA network architecture and the efficiency of our designed GFD protocol.**

***Index Terms*—UAV communications, file dispatching, NOMA, D2D**

I. Introduction

Recently, the application of unmanned aerial vehicles (UAVs) has an explosive growth in various fields, such as film and television, meteorological observation, and military reconnaissance [1]. In addition to these applications, UAV-assisted communications have been of particular interest owing to its significant advantages. The UAVs can be flexibly deployed or recycled when working as mobile base stations (MBSs) for file dispatching [2]. In the literature, the problems of the UAV-assisted communications have been studied from different perspectives [3], [4]. In [3], the authors obtained an optimized trajectory design that makes the UAV take a short time duration to complete the mission. Authors in [4] studied a multi-hop relay system with multiple UAVs as relays, and they jointly optimized the trajectories and transmit power.

Power domain non-orthogonal multiple access (NOMA) is a promising key multiple access technology in the 5th-generation (5G) communication systems [5]. The main idea of NOMA is to realize multiple access through different power levels via the same time-frequency resource block (RB), which can improve the spectral efficiency and access quantity [6]. Since NOMA is suitable for the future system deployment [7], it becomes fashionable to adopt NOMA in UAV-assisted communication networks for file dispatching. In [8], the authors studied the problem of maximizing the sum rate of UAV-assisted NOMA networks through an optimized trajectory of the UAV and precoding vectors of the NOMA base station (BS). In [9], the UAV's placement issue was studied with the aid of machine learning techniques in the UAV-NOMA networks.

In this paper, we investigate the mission latency minimization problem of UAV-assisted file dispatching in a large-scale network. To this end, we apply NOMA in the multicast service of the file dispatching from the UAV to the ground users (GUEs). Besides, the requested data files are divided into different file blocks (FBs), so that the GUEs can share their received FBs using device-to-device (D2D) communications technique [10]. With appropriate resource management and power control, the D2D links can reuse the same resources with the NOMA links based on spatial reuse to reduce the transmission load of the NOMA-based file downloading and further reduce the mission latency [11]. Then, we propose a graph-based file dispatching (GFD) protocol in our investigated D2D-enhanced UAV-NOMA network by dividing the problem into three sub-problems. Simulation results verify the efficiency of our proposed GFD protocol.

The remainder of this paper is organized as follows. Section II presents the system model of the proposed D2D-enhanced UAV-NOMA networks and the problem formulation. Section III gives the details of the proposed GFD protocol. In Section IV, the simulation is introduced and evaluated. We finally conclude our work in Section V.

II. System Model and Problem Formulation

A. System Description

As illustrated in Fig. 1, we consider a typical UAV-assisted communication system with M GUEs denoted by $\mathcal{M}$. All the GUEs request for receiving the same W-bit data file. The location of GUE $m \in \mathcal{M}$ is denoted by $\mathbf{w}_m \in \mathbb{R}^{2\times 1}$. In the investigated scenario, one UAV behaves as the transmitter flying over the considered region while dispatching the requested data file. The altitude of the UAV is fixed to H. Assume that the UAV uses a directional antenna, and the projection of

978-1-7281-3106-1/20/$31.00 ©2020 IEEE

Authorized licensed use limited to: TONGJI UNIVERSITY. Downloaded on September 23,2020 at 04:43:23 UTC from IEEE Xplore. Restrictions apply.

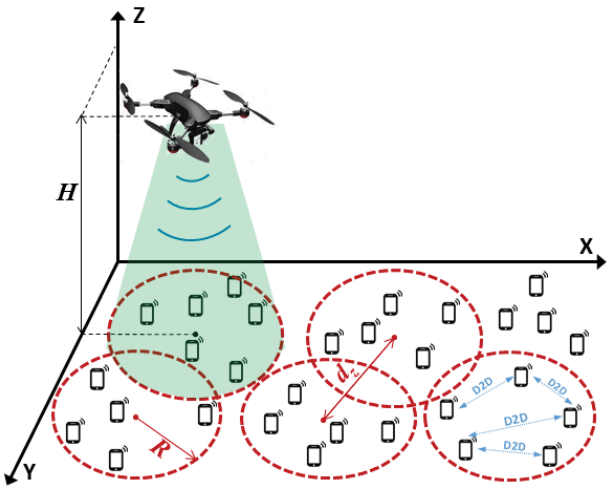

Fig. 1. An illustrated D2D-enhanced UAV-NOMA network.

the beam onto the ground is a circle with radius R, which is highlighted by the red dashed circle in Fig. 1. The set of the Z coverage circles is denoted by $\mathcal{Z}$. d_z is the distance between two circle centers. The UAV's trajectory projected onto the ground with respect to time t is denoted by $\mathbf{q}(t)\in\mathbb{R}^{2\times1}$, and the horizontal flying speed is v m/s.

In our proposed UAV-NOMA system, the data file can be divided into F different FBs, denoted by $\mathcal{F}$, and distributed to different GUEs using NOMA in the NOMA phase. After that, the GUEs that have different FBs can form U D2D pairs, denoted by $\mathcal{U}$, and share FBs with each other in the D2D phase in order to reduce the total mission latency T_{total} of the UAV. The C RBs, denoted by $\mathcal{C}$, are allocated appropriately to different communication links.

B. Channel Analysis

In our investigated D2D-enhanced UAV-NOMA system, there are two main types of communication links, that is, the UAV-GUE links and the D2D links. Denote $\mathcal{H}_m$ and $\mathcal{H}_u$ as the channel coefficient between the UAV and GUE m and between the GUEs in D2D pair $u\in\mathcal{U}$, respectively.

Typically, the UAV-GUE links consist of a line-of-sight (LoS) link and many independent links, so the channel can be characterized as a Rician fading model [3], [12]. Thus,

$$\mathcal{H}_m=\sqrt{\beta_0 d_m^{-\alpha}}\left\{\sqrt{\frac{\kappa_m}{\kappa_m+1}}g_m^{main}+\sqrt{\frac{1}{\kappa_m+1}}g_m^{scatter}\right\} \quad (1)$$

where β_0 denotes the channel power gain at a unit distance, α denotes the path loss factor, and κ_m denotes the Racian factor. g_m^{main} is the channel component of LoS link with $|g_m^{main}|=1$. $g_m^{scatter}$ denotes the channel component of the scattering link, which is a circular symmetric complex Gaussian random variable with $g_m^{scatter}\sim\mathcal{CN}(0,\sigma^2)$. And d_m is the distance between the UAV and GUE m at time t, which is given as

$$d_m=\sqrt{\|\mathbf{q}(t)-\mathbf{w}_m\|^2+H^2}. \quad (2)$$

As for the D2D links, the GUEs in one D2D pair may also have a LoS link between them, and thus the channel of D2D links can be characterized as a Rician fading model as well. Denote $\mathcal{H}_u$ as the channel coefficient between the GUEs in D2D pair $u\in\mathcal{U}$. Then, we obtain the expression of $\mathcal{H}_u$ by replacing the coefficients d_m, κ_m, g_m^{main}, and $g_m^{scatter}$ in Eq. (1) by d_u, κ_u, g_u^{main}, and $g_u^{scatter}$, respectively. d_u denotes the distance between GUE $u_1\in\mathcal{U}$ and $u_2\in\mathcal{U}$ in D2D pair u, which is given by $d_u=\|\mathbf{w}_{u1}-\mathbf{w}_{u2}\|$, where $\mathbf{w}_{u1}$ and $\mathbf{w}_{u2}$ are the locations of u_1 and u_2, respectively.

C. Problem Formulation

The set of the E NOMA groups is denoted by $\mathcal{E}$, and we assume that there are Q GUEs in each NOMA communication group. Note that $M=Q\times E$. In each coverage area, the UAV dynamically chooses GUEs (based on the NOMA principle) to set up NOMA groups, and sends different FBs with different power to the GUEs. Meanwhile, the GUEs can share different FBs using D2D via appropriate RB to minimize total mission latency T_{total}. As a result, the investigated problem can be divided into three parts.

(1) UAV Trajectory Optimization: The center of each UAV's coverage area can be regarded as a mobile base station point (MBSP). The UAV has to fly over all the Z MBSPs and cover as many GUEs as possible at each MBSP. Hence, our objective here is to determine the locations of MBSPs reasonably, and then schedule the visiting order so as to minimize the total flying time t_f. The flying time minimization problem can be expressed as

$$(G1): \quad \min \quad t_f=\sum_{z\in\mathcal{Z}}\frac{d_z}{v} \quad (3a)$$

$$\|\mathbf{w}_m^z-\mathbf{w}_z\|\le R,\quad \forall z\in\mathcal{Z} \quad (3b)$$

where d_z denotes the distance between two MBSPs, given by $\|\mathbf{w}_{z1}-\mathbf{w}_{z2}\|$, $\mathbf{w}_z\in\mathbb{R}^{2\times1}$ denotes the location of the MBSP in coverage $z\in\mathcal{Z}$, and $\mathbf{w}_m^z\in\mathbb{R}^{2\times1}$ denotes the location of the GUE within z. Eq. (3b) ensures that all the GUEs are traversed by the UAV.

(2) NOMA Group Construction: In NOMA group $e\in\mathcal{E}$, the received signal on RB $c\in\mathcal{C}$ at user $m_q\in\mathcal{M}$ $(q=1,2,\cdots,Q)$ can be expressed as

$$y_{m_q}^e=\sum_{i=1}^{Q}\mathcal{H}_{m_q}\sqrt{a_{m_i}^e P_e}x_{m_i}+\sum_{u\in\mathcal{U}}\eta_e^u\mathcal{H}_{u_q}\sqrt{P_u}x_u+\zeta_{m_q} \quad (4)$$

where $\mathcal{H}_{m_q}$ and $\mathcal{H}_{u_q}$ denote the channel gains from the UAV and the transmitter of D2D pair $u\in\mathcal{U}$ to the GUE m_q, respectively, which are given in Section II-B. $a_{m_i}^e$ denotes the transmit power allocation coefficient of NOMA with $0<a_{m_i}^e<1$. P_e and P_u denote the total transmit power allocated by the UAV to each NOMA group and the GUE's transmit power, respectively. x_{m_i} and x_u denote the transmit signals from the UAV and D2D pair u, respectively. ζ_{m_q} is the additive white Gaussian noise (AWGN) with variance σ^2. The RB allocation indicator is denoted by η_e^u. $\eta_e^u=1$ when e and u are working through the same RB simultaneously, otherwise, $\eta_e^u=0$.

Assume that the Q GUEs in NOMA group e are sorted in order of $d_{m_1}<d_{m_2}<\cdots<d_{m_Q}$. Considering the interference caused by the superposition signals of NOMA

Authorized licensed use limited to: TONGJI UNIVERSITY. Downloaded on September 23,2020 at 04:43:23 UTC from IEEE Xplore. Restrictions apply.

and the interference caused by the resource reusing by D2D pairs, the received SINR at m_q can be given as

$$\varphi_{m_q} = \frac{\left|\mathcal{H}_{m_q}\right|^2 P_e a^e_{m_q}}{P_e \left|\mathcal{H}_{m_q}\right|^2 \sum_{i=1}^{q-1} a^e_{m_i} + \sum_{u\in\mathcal{U}} \eta^u_e \left|\mathcal{H}_{u_q}\right|^2 P_u + \sigma^2}. \quad (5)$$

Based on Eq. (5) and the Shannon formula, we can obtain the transmission rate of m_q as

$$\mathfrak{R}_{m_q} = BW_e \cdot \log_2(1+\varphi_{m_q}) \quad (6)$$

where BW_e denotes the bandwidth allocated by the UAV to NOMA group e.

Therefore, the objective in this part is to maximize the minimum rate of all the UAV-GUE links, and thus reduce the time of the UAV's file dispatching, which can be given as

$$(G2): \quad \max \quad \min\{\mathfrak{R}_{m_q}\} \quad (7a)$$

$$\text{s.t.} \quad \sum_{q=1}^{Q} a^e_{m_q} = 1, \quad \forall e \in \mathcal{E} \quad (7b)$$

$$\sum_{e\in\mathcal{E}} P_e \le P_{uav} \quad (7c)$$

$$Q \ge F \quad (7d)$$

$$\varphi_m \ge \varphi_0, \quad \forall m \in \mathcal{M} \quad (7e)$$

where Eq. (7b) limits the total power allocated to the GUEs within each NOMA group to P_e, Eq. (7c) limits the total power allocated to all the NOMA groups to P_{uav}, and Eq. (7d) ensures that all the FBs are available within each NOMA group. φ_m denotes the SINR received by GUE $m \in \mathcal{M}$. And Eq. (7e) ensures that the received SINR at each GUE is greater than the demodulation threshold φ_0.

(3) Phase Switching Control: The GUEs with different FBs can be chosen to work in the D2D phase for file sharing on the same RBs used by NOMA links. It is vital to ensure that no substantial interference exists between D2D and NOMA links. When the received SINR at NOMA users is analyzed, the influence of D2D links has been already taken into account as shown in Eq. (5). Correspondingly, when the GUEs are working in the D2D phase, the SINR φ_u received by the receiver in D2D pair u are given by

$$\varphi_u = \frac{|\mathcal{H}_u|^2 P_u}{P_{u'} \cdot \sum_{u'\in\mathcal{U}, u'\ne u} \eta^{u'}_e |\mathcal{H}_{u'}|^2 + \sum_{e\in\mathcal{E}} \eta^u_e |\mathcal{H}_u|^2 P_e + \sigma^2} \quad (8)$$

where $\mathcal{H}_{u'}$ denotes the channel gain from the transmitter of D2D pair $u' \in \mathcal{U}$ ($u' \ne u$) to the receiver of D2D pair u, $P_{u'}$ denotes the transmit power of u', and ζ_u is the AWGN with variance σ^2. $\eta^{u'}_e$ is the RB allocation indicator with the same meaning of η^u_e, that is, $\eta^{u'}_e = 1$ when e and u' are working through the same RB simultaneously, otherwise, $\eta^{u'}_e = 0$.

The transmission rate of D2D pair u can be expressed as

$$\mathfrak{R}_u = BW_u \cdot \log_2(1+\varphi_u) \quad (9)$$

where BW_u denotes the bandwidth allocated to D2D pair u.

Therefore, the objective here is to maximize the minimum rate of all the D2D pairs, which can be given as

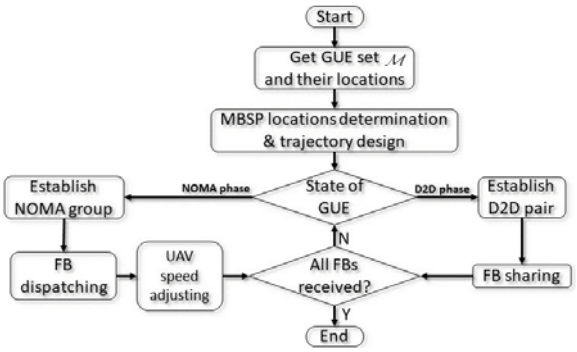

Fig. 2. Flow diagram of the GFD protocol.

$$(G3): \quad \max \quad \min\{\mathfrak{R}_u\} \quad (10a)$$

$$\text{s.t.} \quad \varphi_u \ge \varphi_0, \quad \forall u \in \mathcal{U} \quad (10b)$$

$$\sum_{c\in\mathcal{C}} \eta^u_e \le 1, \quad \forall e \in \mathcal{E}, u \in \mathcal{U} \quad (10c)$$

$$\sum_{e,u} \eta^u_e \le \rho, \quad \forall c \in \mathcal{C} \quad (10d)$$

where Eq. (10b) guarantees each GUE working in the D2D phase to have a required quality of service (QoS). Eq. (10c) limits the number of RBs allocated to each communication group. Eq. (10d) restricts the amount of communication links that can reuse the same RB at the same time to ρ.

Then, the time of NOMA transmission t^z_N and D2D transmission t^z_D can be expressed as $t^z_N = W/\{F \cdot \min(\mathfrak{R}_{m_q})\}$ and $t^z_D = W/\{F \cdot \min(\mathfrak{R}_u)\}$, respectively.

Therefore, the ultimate objective based on the above analysis can be given as

$$(G): \quad \min \quad T_{total} = \sum_{z\in\mathcal{Z}} \max\{t^z_f, t^z_N\} \quad (11a)$$

$$\text{s.t.} \quad \sum_{z\in\mathcal{Z}} t^z_D \le T_{total} \quad (11b)$$

$$\text{Eq. (3b), (7b)}-\text{(7e), (10b)}-\text{(10d)}$$

where Eq. (11b) ensures that the D2D phase can be completed before the UAV completes its flight.

III. Graph-Based File Dispatching Protocol

In order to solve problem G, we propose the GFD protocol in this section. Similar to the problem formulation, the GFD protocol will be described in three parts in the following, and the flow chart of the GFD protocol is provided in Fig. 2.

A. UAV Trajectory Optimization

(1) MBSP Location Determination: The location determination problem of the MBSPs is a typical geometric disk cover one [13], and we solve this problem by applying the spiral MBS placement (SMBSP) algorithm proposed in [14].

First, all the outermost GUEs are categorized as boundary GUEs $\mathcal{GUE}_{bo}$ and arranged in counterclockwise order. The rest of the GUEs that are not on the boundary naturally become inner GUEs $\mathcal{GUE}_{in}$. A boundary GUE $m_{bo} \in \mathcal{GUE}_{bo}$ is randomly selected as the first MBSP z at the beginning. Next, the location of MBSP z is adjusted so that it can cover as many other boundary GUEs as possible while guaranteeing

Authorized licensed use limited to: TONGJI UNIVERSITY. Downloaded on September 23,2020 at 04:43:23 UTC from IEEE Xplore. Restrictions apply.

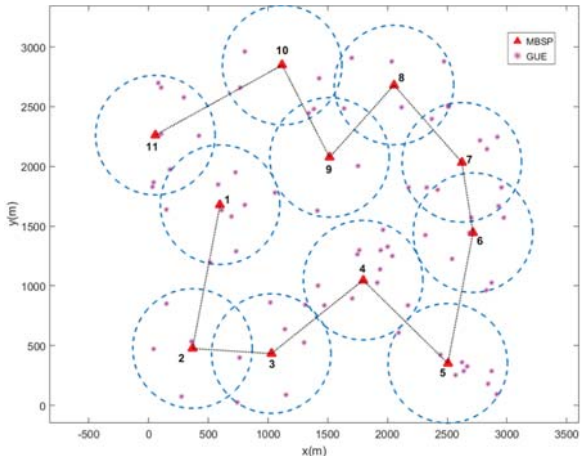

Fig. 3. An example of the optimized UAV trajectory.

that GUE m_{bo} is covered. Then, the location of MBSP z will be adjusted again so as to cover the inner GUEs as many as possible on the premise of guaranteeing the currently covered boundary GUEs. And now, the first MBSP is located. After that, the new boundary GUEs are re-found in all uncovered GUEs. The above processes are repeated until all the GUEs are covered. The detailed operation and the derivations of the SMBSP algorithm with the complexity of $\mathcal{O}(M^2 \log M)$ can be found in [14].

(2) Flying Path Scheduling: After the locations of MBSPs are determined, the next step is to schedule the visiting order of all MBSPs so as to minimize the total flying distance. This problem can be modeled as a traveling salesman (TSM) problem, which is a classical NP-Hard problem [15]. In this paper, we apply the solver-based TSM (S-TSM) algorithm [16], which is a sub-optimal method, to solve the TSM problem. The detailed procedure of the S-TSM algorithm is given in [16] with the complexity of $\mathcal{O}(Z^2)$. An example of the optimized UAV trajectory is shown in Fig. 3.

In Fig. 3, the blue dashed circle denotes the coverage of each MBSP with the radius of R. The UAV will fly over the first MBSP to dispatch FBs to the GUEs within its coverage, and then fly to the next MBSP sequentially.

B. NOMA Group Construction

When the UAV flies in coverage z, it divides all the GUEs within the coverage of $z \in \mathcal{Z}$ into E NOMA groups based on their CSI, and allocates power to different GUEs with a fixed power allocation coefficient. To solve the NOMA user grouping problem in $G2$, we propose a hypergraph-based grouping (HG-G) algorithm. The HG-G algorithm introduces the concept of hypergraph [7], [17].

Let $\mathcal{HG} = (\mathcal{HV}, \mathcal{HE})$ be a hypergraph, where $\mathcal{HV}$ is the set of vertices representing the GUEs within the coverage of z, and $\mathcal{HE}$ is the set of hyperedges representing the matching relationships between vertices. Q GUEs are connected by hyperedge $he \in \mathcal{HE}$ forming a NOMA group e. And the weight ω of hyperedge he is set to be the minimum SINR of the Q GUEs in NOMA group e. Here, the NOMA user grouping problem can be modeled as a valid matching in the weighted hypergraph $\mathcal{HG}$.

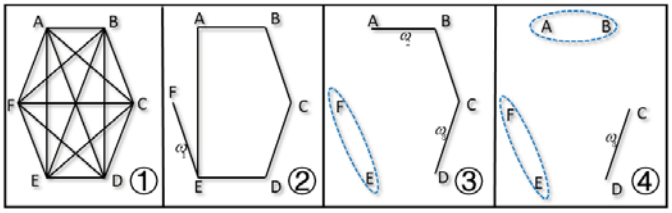

Fig. 4. An example of the HG-G algorithm with $Q = 2$.

Definition 1: In a hypergraph $\mathcal{HG} = (\mathcal{HV}, \mathcal{HE})$, **strongly delete** a vertex $vx \in \mathcal{HV}$ from $\mathcal{HG}$ means removing all the hyperedges containing vx from $\mathcal{HE}$ and then removing vx from $\mathcal{HV}$.

First, all the hyperedges are arranged in the descending order of their weights. Then, the hyperedge with the smallest weight is deleted sequentially until a vertex $vx_1 \in \mathcal{HV}$ that connected by only one hyperedge $he_1 \in \mathcal{HE}$ comes up. Thus, vertex vx_1 and the other vertices contained in he_1 form a NOMA group naturally.

Next, vx_1 and the other vertices contained in he_1 are strongly deleted from $\mathcal{HG}$. Then, vx_1 and he_1 are updated by finding the vertex again that connected by only one hyperedge. The finding and deleting cyclic operation will be repeated until all the hyperedges in the hypergraph have been deleted. Finally, the sub-optimal NOMA groups satisfying problem $G2$ are obtained.

Fig. 4 illustrates an example of the HG-G algorithm with $Q = 2$. A hypergraph will degenerate into an ordinary graph when each hyperedge contains only two vertices. As we can see in Fig. 4-①, the hypergraph (graph) is constructed with 6 users and the hyperedges (edges) represent the potential NOMA groups. Vertex F connected by only one edge appears, after all the edges with the minimum weight are deleted sequentially, which is shown in Fig. 4-②. Then, we can make the decision that user F and E can form a NOMA group. The graph becomes what is shown in Fig. 4-③ when vertices F and E are strongly deleted. We can also see in Fig. 4-③ that, both vertices A and D are connected by only one edge. Assume that $\omega_2 > \omega_3$, and thus we choose vertices A and B to form a NOMA group leaving vertices C and D form a NOMA group naturally as shown in Fig. 4-④.

The detailed procedure of the HG-G algorithm is summarized in Algorithm 1. And because of the double loop and the sorting process in the algorithm, the worst-case complexity of the HG-G algorithm is $\mathcal{O}(E^2)$.

C. Phase Switching Control

The GUEs will start to work in the D2D phase as long as they has finished FB receiving through NOMA. We use $z \in \mathcal{Z}$ to represent the circle of the coverage of each MBSP as well. GUEs with different FBs are paired until all the GUEs get a whole data file. We apply graph theory again.

We construct an ordinary graph $\mathcal{G} = (\mathcal{V}, \mathcal{ED})$ in which the vertices represent the GUEs and the edges represent that the two connected vertices have different FBs to share. The weight of each edge represents the transmission rate between the GUEs in each D2D pair without interference. Then, the edge with the heaviest weight is selected as the

Authorized licensed use limited to: TONGJI UNIVERSITY. Downloaded on September 23,2020 at 04:43:23 UTC from IEEE Xplore. Restrictions apply.

Algorithm 1: HG-G Algorithm

Input: $\mathcal{Z}, \mathbf{w}_m^z$.
Initialization: $i \leftarrow 1$.
Construct hypergraph $\mathcal{HG} = (\mathcal{HV}, \mathcal{HE})$.
$\mathcal{HE}_{sort}$=sort($\mathcal{HE}$,'descent').
while $\mathcal{HG} \neq \emptyset$ **do**
  Find vx_1 that connected by he_1 only.
  while *length*(vx_1)$= 0$ **do**
    Delete the hyperedge with the smallest ω
  end
  if *length*(vx_1)> 1 **then**
    Find the vertex vx_1 with the biggest ω.
    Update vx_1 and he_1.
  end
  if *length*(vx_1)$= 1$ **then**
    $e_i \leftarrow e_i \cup he_1$, then strongly delete vx_1.
    $i \leftarrow i + 1$.
  end
end
Output: $\mathcal{E}$.

currently established D2D pair sequentially, and the two vertices connected by this edge are strongly deleted from $\mathcal{G}$. After all the D2D pairs are selected, a round of FB sharing is completed. Then, a new graph is reconstructed based on the current condition and the above processes are repeated so that all the FBs can be shared.

Algorithm 2: Graph-based D2D Pairing Algorithm

Input: $\mathcal{M}$.
Initialization: $Flag \leftarrow 1$.
while $Flag = 1$ **do**
  Construct graph $\mathcal{G} = (\mathcal{V}, \mathcal{ED})$.
  Calculate the weight of each edge.
  while $\mathcal{ED} \neq \emptyset$ **do**
    Find the edge ed with the largest weight.
    $\mathcal{U} \leftarrow \{ed\}$.
    Strongly delete the vertices connected by ed.
  end
  Call Algorithm 3.
  if *No GUE needs FBs* **then**
    $Flag \leftarrow 0$
  end
end
Output: $\mathcal{U}$.

In the D2D phase, different D2D pairs are allowed to share the same RB if the mutual interference between them is less than threshold Θ_φ. And different circles can share RBs when the distance between the corresponding MBSPs is greater than threshold $\Theta_d > 2R$. The proposed graph-based D2D pairing algorithm is provided in Algorithm 2.

IV. Numerical Results and Discussions

Our simulation setup considers a 3km×3km square area covered by one UAV. And we randomly arrange the M GUEs in the considered area on the ground. For simplicity and

Algorithm 3: RB Reusing Algorithm

Input: $\mathcal{M}$.
Initialization: $Flag \leftarrow 1$, $\eta_e^u \leftarrow 0 (\forall u \in \mathcal{U})$.
Construct graph $\mathcal{G}' = (\mathcal{V}', \mathcal{ED}')$ in which the vertices represent D2D pairs and the edges represent the interference relationships.
Calculate the weight ω' of each edge which means the interference between the D2D pairs.
for $u = 1 : U$ **do**
  if $\omega_u' > \Theta_\varphi$ **then**
    $\eta_e^u \leftarrow 1$
  end
end
Output: $\mathcal{U}, \eta_e^u (\forall u \in \mathcal{U})$.

TABLE I
System Parameters

Parameters	Value
Carrier frequency	2 GHz
Total Bandwidth	1 MHz
RB Bandwidth	10 KHz
Path Loss Factor α	2.6
Rician Factor	$\kappa_m = 2$, $\kappa_u = 1.5$
Reference Channel Gain β_0	-40 dB
Noise Power σ^2	-109 dBm
Noise Figure	10 dB
UAV Transmit Power P_{UAV}	10 dBm
UAV Speed v	50 m/s
UAV Altitude H	100 m
UAV Coverage Radius R	300 m
GUE Transmit Power P_u	10 dBm
File Size W	2 Mbits
Updating Interval τ	1 ms

without loss of generality, we set $Q = F = 2$, which means that each NOMA group has two receivers and the data file is divided into two FBs. The UAV can dispatch the two FBs to the two GUEs within the same NOMA group. All the other parameters applied in our simulation in MATLAB are summarized in Table I.

As a baseline, we employ different file dispatching schemes in the investigated scenario for UAV-assisted file dispatching. Fig. 5 compare the total time of the UAV to complete the data file dispatching as the number of GUEs increases with different file dispatching schemes. The scheme "noNOMAnoD2D" represents that the UAV uses OFDMA to dispatch files, and ensure that each GUE receives a complete data file. As we can see, the noNOMAnoD2D scheme is much less efficient than our proposed NOMA+D2D scheme. And our proposed GFD protocol will have more advantages especially when the number of the GUEs increases. The scheme "onlyNOMAnoD2D" represents that the UAV exploits NOMA to dispatch files without the assistance of D2D. In this case, the UAV has to send all FBs to each GUE through NOMA. Obviously, the onlyNOMAnoD2D scheme takes less time than the noNOMAnoD2D scheme, due to the application of NOMA. However, the UAV has to wait for the completion of all GUE's data-receiving because of the lack of D2D.

Afterwards, we analyze the influence of the UAV coverage radius R on the mission latency with $M = 80$, which is shown in Fig. 6. As we can see that, the mission latency of our proposed GFD protocol with the NOMA+D2D scheme

Authorized licensed use limited to: TONGJI UNIVERSITY. Downloaded on September 23,2020 at 04:43:23 UTC from IEEE Xplore. Restrictions apply.

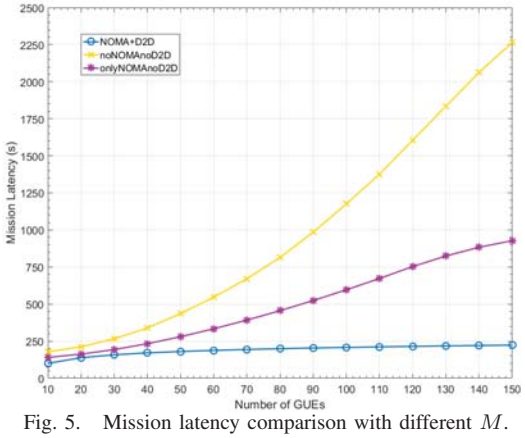

Fig. 5. Mission latency comparison with different M.

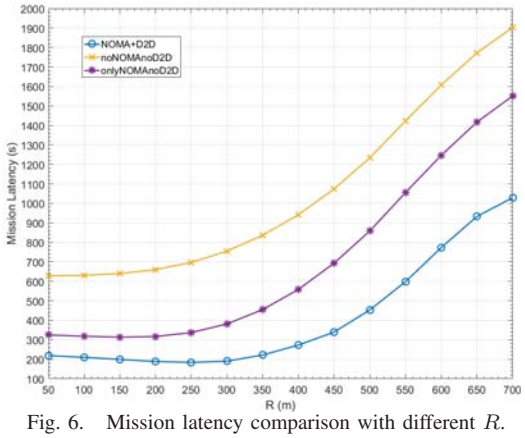

Fig. 6. Mission latency comparison with different R.

first decreases and then increases with the increase of R. This is because the UAV can only cover a very small area at a time when R is small, and more MBSPs are needed to complete the mission. With the increase of R, the number of MBSPs can be reduced. Hence, the UAV's flying path is shortened and more GUEs can be covered at the same time, resulting in a smaller T_{total}. However, although the number of MBSPs decreases with the further increasing of R, the GUEs that are far away from the UAV are also included in the coverage. Thus, the transmission rate becomes lower, and the UAV has to fly at a lower speed to ensure the correct file dispatching, resulting in an increased T_{total}. At the same time, it can be seen that the mission latency of the noNOMAnoD2D scheme almost keeps increasing with the increase of R. This is because the noNOMAnoD2D scheme does not have any assistance, and thus, the UAV has to wait for the finish of file transmission, no matter how far away the GUE is from the UAV and how bad the channel state is. While, the efficiency of the onlyNOMAnoD2D scheme is between that of the other two schemes because of the use of NOMA.

V. Conclusions

This paper investigated the mission latency minimization problem in the UAV-assisted communication networks. In order to improve the network performance, we proposed a D2D-enhanced UAV-NOMA network architecture, and resource sharing based on spatial reuse were employed. Then, we further proposed the GFD protocol to solve the optimization problem efficiently by dividing the problem into three sub-problems. Simulation results verified the efficiency of our designed GFD protocol in improving the performance of the proposed network.

Acknowledgement

This work was in part supported by the Ministry National Key Research and Development Project under Grant 2017YFE0121400, the National Natural Science Foundation of China under Grant 61901302, Guangdong Key R&D Project under Grant 2018B030338001, the open research fund of Key Laboratory of Wireless Sensor Network & Communication under Grant 2017003, Shanghai Institute of Microsystem and Information Technology, Chinese Academy of Sciences, the open research fund of National Mobile Communications Research Laboratory, Southeast University (No. 2020D01), and the National Science Foundation under Grant CPS-1932413 and ECCS-1935915.

References

[1] S. Zhang, Y. Zeng, and R. Zhang, "Cellular-enabled UAV communication: A connectivity-constrained trajectory optimization perspective," *IEEE Trans. Commun.*, vol. 67, no. 3, pp. 2580–2604, Mar. 2019.

[2] X. Yuan *et al.*, "Capacity analysis of UAV communications: cases of random trajectories," *IEEE Trans. Veh. Technol.*, vol. 67, no. 8, pp. 7564–7576, Aug. 2018.

[3] Y. Zeng, X. Xu, and R. Zhang, "Trajectory design for completion time minimization in UAV-enabled multicasting," *IEEE Trans. Wireless Commun.*, vol. 17, no. 4, pp. 2233–2246, Apr. 2018.

[4] G. Zhang, H. Yan, Y. Zeng, M. Cui, and Y. Liu, "Trajectory optimization and power allocation for multi-hop UAV relaying communications," *IEEE Access*, vol. 6, pp. 48566–48576, Aug. 2018.

[5] Z. Ding *et al.*, "A survey on non-orthogonal multiple access for 5G networks: Research challenges and future trends," *IEEE J. Sel. Areas Commun.*, vol. 35, no. 10, pp. 2181–2195, Oct. 2017.

[6] Z. Ding, Z. Yang, P. Fan, and H. V. Poor, "On the performance of non-orthogonal multiple access in 5G systems with randomly deployed users," *IEEE Sig. Process. Lett.*, vol. 21, no. 12, pp. 1501–1505, Dec. 2014.

[7] B. Wang *et al.*, "Interference hypergraph-based 3D matching resource allocation protocol for NOMA-V2X networks," *IEEE Access*, vol. 7, pp. 90789–90800, Jul. 2019.

[8] N. Zhao *et al.*, "Joint trajectory and precoding optimization for UAV-assisted NOMA networks," *IEEE Trans. Commun.*, vol. 67, no. 5, pp. 3723–3735, May. 2019.

[9] Y. Liu *et al.*, "UAV communications based on non-orthogonal multiple access," *IEEE Wireless Commun.*, vol. 26, no. 1, pp. 52–57, Feb. 2019.

[10] R. Zhang, X. Cheng, L. Yang, and B. Jiao, "Interference graph-based resource allocation (InGRA) for D2D communications underlaying cellular networks," *IEEE Trans. Veh. Technol.*, vol. 64, no. 8, pp. 3844–3850, Aug. 2015.

[11] X. Cheng, L. Yang, and X. Shen, "D2D for intelligent transportation systems: A feasibility study," *IEEE Trans. Intell. Trans. Syst.*, vol. 16, no. 4, pp. 1784–1793, Jan. 2015.

[12] X. Cheng and Y. Li, "A 3-D geometry-based stochastic model for UAV-MIMO wideband nonstationary channels," *IEEE Internet Things J.*, vol. 6, no. 2, pp. 1654–1662, Apr. 2019.

[13] A. Srinivas, G. Zussman, and E. Modiano, "Construction and maintenance of wireless mobile backbone networks," *IEEE/ACM Trans. Netw.*, vol. 17, no. 1, pp. 239–252, Feb. 2009.

[14] J. Lyu, Y. Zeng, R. Zhang, and T. J. Lim, "Placement optimization of UAV-mounted mobile base stations," *IEEE Commun. Lett.*, vol. 21, no. 3, pp. 604–607, Mar. 2017.

[15] G. Laporte, "The traveling salesman problem: An overview of exact and approximate algorithms," *EUR. J. Oper. Res.*, vol. 59, no. 2, pp. 231–247, Jun. 1992.

[16] *Traveling Salesman Problem: Solver-Based*. Accessed: Jul. 22, 2017. [Online]. Available: https://www.mathworks.com/help/optim/ug/travelling-salesman-problem.html

[17] S. Sarkar and K. N. Sivarajan, "Hypergraph models for cellular mobile communication systems," *IEEE Trans. Veh. Technol.*, vol. 47, no. 2, pp. 460–471, May 1998.

Authorized licensed use limited to: TONGJI UNIVERSITY. Downloaded on September 23,2020 at 04:43:23 UTC from IEEE Xplore. Restrictions apply.